Popular Summary:

"Modulation of Atlantic Aerosols by the Madden-Julian Oscillation"

Tian, B., D.E. Waliser, R.A. Kahn, and S. Wong, 2010.

J. Geophys. Res., submitted.

Much like the better-known El Nino–Southern Oscillation, the Madden-Julian Oscillation (MJO) is a global-scale atmospheric phenomenon. The MJO involves periodic, systematic changes in the distribution of clouds and precipitation over the western Pacific and Indian oceans, along with differences in wind intensity over even more extensive areas, including the north and sub-tropical Atlantic Ocean. The lead authors of this paper developed a sophisticated mathematical technique for mapping the spatial and temporal behavior of changes in the atmosphere produced by the MJO. In a previous paper, we applied this technique to search for modulation of airborne particle amount in the eastern hemisphere associated with the "wet" (cloudy) vs. "dry" phases of the MJO. The study used primarily AVHRR, MODIS, and TOMS satellite-retrieved aerosol amount, but concluded that other factors, such as cloud contamination of the satellite signals, probably dominated the observed variations.

The current paper looks at MJO modulation of desert dust transport eastward across the Atlantic from northern Africa, a region much less subject to systematic cloud contamination than the eastern hemisphere areas studied previously. In this case, a distinct aerosol signal appears, showing that dust is transported westward much more effectively during the MJO phase that favors westward-flowing wind, and such transport is suppressed when the MJO reduces these winds. Aside form the significant achievement in identifying such an effect, the result implies that an important component of global dust transport can be predicted based on the phase of the MJO. As a consequence, the impact of airborne dust on storm development in the Atlantic, and on dust deposition downwind of the desert sources, can also be predicted and more accurately modeled.

Modulation of Atlantic Aerosols by the Madden-Julian Oscillation

Baijun Tian[1], Duane E. Waliser[1], Ralph A. Kahn[2], and Sun Wong[1]

[1]*Jet Propulsion Laboratory, California Institute of Technology, Pasadena, CA*

[2]*NASA Goddard Space Flight Center, Greenbelt, MD*

Correspondence to: Baijun Tian (baijun.tian@jpl.nasa.gov)

Abstract

Our previous study found large intra-seasonal variations in satellite-derived aerosol products over tropical Atlantic Ocean associated with the Madden-Julian Oscillation (MJO). This study aims to investigate the physical mechanism of these aerosol anomalies through analyzing aerosol optical thickness (AOT) from the MODIS instrument on Aqua satellite and low-level (850-hPa) horizontal winds from NCEP/NCAR reanalysis. Our analysis indicates that when enhanced MJO convection is located over the equatorial Indian Ocean (western Pacific), persistent low-level westerly (easterly) anomalies over the equatorial Atlantic reduce (enhance) the low-level westward aerosol transport from Africa and induce negative (positive) AOT anomalies over the equatorial Atlantic. These results indicate that the MJO modulates the Atlantic aerosol concentration through its influence on the Atlantic low-level zonal wind anomalies and westward aerosol transport from Africa. This study implies that Atlantic aerosol concentration might have predictable components with lead times of 2-4 weeks given the predictability of the MJO.

1. Introduction

The Madden-Julian Oscillation (MJO) [*Madden and Julian*, 1971; 1972] is the dominant form of the intra-seasonal (30–90 day) variability in the tropical atmosphere and is characterized by slow (~5 m s^{-1}) eastward-propagating, large-scale oscillations in the tropical deep convection and baroclinic winds, especially over the warmest tropical waters in the equatorial Indian Ocean and western Pacific, during boreal winter (November-April), when the Indo-Pacific warm pool is centered near the equator [*Lau and Waliser*, 2005; *Zhang*, 2005]. It has been well documented that the MJO can impact numerous physical weather and climate phenomena over the globe. However, the impact of the MJO on atmospheric composition is only beginning to be realized [e.g., *Li et al.*, 2010; *Tian et al.*, 2007; *Weare*, 2010; *Wong and Dessler*, 2007; *Ziemke and Chandra*, 2003].

Recently, *Tian et al.* [2008] examined the aerosol variability related to the MJO using multiple, global satellite aerosol products including aerosol index (AI) from the Total Ozone Mapping Spectrometer (TOMS) on Nimbus-7 satellite, and aerosol optical thickness (AOT) from the Moderate Resolution Imaging Spectroradiometer (MODIS) on Terra satellite and the Advanced Very High Resolution Radiometer (AVHRR) on NOAA satellites. That analysis indicated large intra-seasonal variations in the aerosol products over the whole Tropics (see Figures 2 and 4 of *Tian et al.* [2008]). {Baijun – I suggest this rewording because the variations were in the aerosol *products*, but likely not in the actual aerosols, in this case.} Over the tropical Indian Ocean and western Pacific where MJO convection is active and the background aerosol level is low, a strong inverse linear relationship between the TOMS AI and rainfall anomalies, but a weaker, less coherent

46 *positive* correlation between the MODIS/AVHRR AOT and rainfall anomalies, were
47 found. Although a number of plausible mechanisms for these relationships exist, the
48 exact causes are still to be determined.

49 Over the equatorial Atlantic Ocean and Africa where MJO convection is weak but
50 the background aerosol level is high, the spatial and temporal patterns of TOMS AI and
51 MODIS AOT anomalies are similar. When the enhanced MJO convection is located over
52 the equatorial Indian Ocean (western Pacific), the aerosol anomalies over the equatorial
53 Atlantic Ocean and Africa are negative (positive). Since the MJO convection and
54 associated cloud anomalies are rather weak over the equatorial Atlantic Ocean and
55 Africa, the cloud contamination effect for the AOT MJO anomalies should be weak too
56 over this region [*Tian et al.*, 2008]. However, how the MJO generates these aerosol
57 variations over the equatorial Atlantic Ocean and Africa was not addressed in *Tian et al.*
58 [2008]. The purpose of the present study is to investigate how the MJO generates these
59 intra-seasonal aerosol variations over the equatorial Atlantic Ocean and modulates the
60 Atlantic aerosol concentration.

61 Given the potential predictability of the MJO extending to 2-4 weeks [e.g.,
62 *Waliser*, 2005], if the MJO does influence the Atlantic aerosols, then the Atlantic aerosol
63 concentration may be predictable with lead times of 2-4 weeks, which in turn may lend
64 important guidance to prediction of air quality, dust storm activity, and ocean nutrient
65 deposition over the Atlantic Ocean. Furthermore, the modulation of Atlantic aerosol by
66 the MJO will provide an important physical/chemical process to evaluate chemical
67 transport models and help model development. Section 2 describes the data sets and
68 analysis methodology used in this study. Section 3 presents the main results followed by

69 conclusions and discussion in Section 4.

70 **2. Data and methodology**

71 For this study, we use the MODIS/Aqua Collection 5.1 (C051), Level-3 (L3)
72 daily global aerosol product 'Optical_Depth_Land_And_Ocean' (MYD08_D3). The data
73 are on 1° × 1° spatial grids and from 4 July 2002 to 1 June 2009. This aerosol product
74 represents total-column AOT at 0.55 μm over both ocean (best) [*Tanre et al.*, 1997] and
75 land (corrected) except for bright surfaces [*Kaufman et al.*, 1997] based on the 'dark
76 target' algorithm [*Remer et al.*, 2005; 2008]. To characterize the large-scale circulation
77 patterns that transport aerosols, daily horizontal winds from the National Centers for
78 Environmental Prediction/National Center for Atmospheric Research (NCEP/NCAR)
79 reanalysis were used. The wind data have a spatial resolution of 2.5°×2.5° and are from
80 2002 to 2009.

81 For the MJO analysis and composite procedure, we use the multivariate empirical
82 orthogonal function (EOF) method introduced by *Wheeler and Hendon* [2004] and
83 adopted widely by the MJO community [e.g., *Waliser et al.*, 2009]. The comparison of
84 this multivariate EOF method and the extended EOF method used in our previous aerosol
85 study [*Tian et al.*, 2008] has been examined by *Tian et al.* [2010] with the finding that
86 both methods yield similar results for the MJO composite analysis. Briefly, the intra-
87 seasonal anomalies of daily aerosol and wind data were obtained by removing the
88 climatological-mean seasonal cycle and filtering via a 30–90-day band pass filter. Then, a
89 composite MJO cycle (8 phases) was calculated by averaging the daily anomalies that
90 occurred within each phase of the MJO cycle. The MJO phase for each day is determined
91 by the Real-time Multivariate MJO (RMM) index (a pair of PC time series called RMM1

92 and RMM2; available from 1974 to present at
93 http://www.cawcr.gov.au/bmrc/clfor/cfstaff/matw/maproom/RMM/). Figure 1 shows the
94 (RMM1, RMM2) phase space for all days in boreal winter from November 2002 to April
95 2009 and the number of days for each phase of the composite MJO cycle. Only days with
96 strong MJO activity ($RMM1^2+RMM2^2>=1$) are considered. The statistical assessment as
97 to whether a composite mean at each point is different from zero is assessed by the two -
98 sided t test, $t = \sqrt{N}\bar{x}/\sigma$. Here, N is the number of samples in the composite mean and in
99 this case the number of days for each phase of the composite MJO cycle. $\bar{x}$ and σ are the
100 composite mean and standard deviations of the AOT samples for each phase of the
101 composite MJO cycle.

102 **3. Results**

103 Figure 2a shows the climatological mean (2002-2009) boreal winter
104 MODIS/Aqua AOT and NCEP/NCAR 850-hPa horizontal winds over the tropical
105 Atlantic and nearby region (90°W-50°E, 40°S-40°N). In Figure 2a, the strong impact of
106 land surface emission and large-scale horizontal, especially zonal, wind transport are
107 evident in the aerosol distribution. For example, large aerosol loadings are found near the
108 Sahara and Arabian deserts due to strong sources of desert dust and over equatorial
109 Africa and Amazon associated with biomass burning activities [*Kaufman et al.*, 2005].
110 The dominant aerosol feature over the tropical Atlantic is the zonally oriented optically
111 thick aerosol plume centered at 5°N-8°N stretching across the Atlantic. Its magnitude
112 (>0.6) and latitudinal extent (~15°S - 20°N) are greatest over the eastern equatorial
113 Atlantic along the west coast of Africa and gradually decrease westward toward the
114 central and western equatorial Atlantic. It can reach the northeast coast of South America

115 and Amazon basin with sizable AOT values (~0.2). This aerosol plume is the result of the
116 equatorial Atlantic trade winds that transport the mixed Saharan/Sahelian dust and
117 biomass-burning smoke from Africa to the Atlantic Ocean [e.g., *Cakmur et al.*, 2001;
118 *Carlson and Prospero*, 1972; *Huang et al.*, 2010; *Husar et al.*, 1997; *Kaufman et al.*,
119 2005]. Over the midlatitude Atlantic (~40°N/S), there is a relatively high aerosol loading
120 (~0.15) that is associated with the midlatitude westerlies that transport the industrial
121 pollution (sulfate and carbonaceous aerosols) from South and North America to the
122 Atlantic Ocean. Over the subtropical North and South Atlantic (~25°N/S), two high-
123 pressure anticyclones (e.g., Azores high) dominate and the aerosol loading there is very
124 low (~0.05).

125 Figure 2b shows the similar map as Figure 2a except for the 700-hPa
126 NCEP/NCAR horizontal winds. Comparing Figure 2a and 2b indicates that the large-
127 scale circulation patterns are roughly similar between 850 and 700 hPa, such as the
128 equatorial trade winds and subtropical highs. Thus, both wind patterns can explain the
129 gross aerosol distribution pattern. However, there are two notable differences. First, over
130 the Gulf of Guinea, the easterly wind speed is much larger at 700 hPa than at 850 hPa and
131 a correlation analysis indicates that the linear correlation between the mean AOT and
132 westerly wind speed is higher at 700-hPa than at 850 hPa. Thus, the 700-hPa winds may
133 play a more important role in transporting the aerosol over this region. {Includes smoke
134 and some dust.} Second, over the Saharan desert and west coast of Africa near 20°N,
135 northeasterly trade winds dominate at 850 hPa, whereas westerlies are common at 700
136 hPa. Thus, the aerosol (mostly dust) over the west coast of Africa near 20°N is more
137 likely transported by the 850-hPa winds instead of the 700-hPa winds as first noted by

138 *Chiapello et al.* [1995]. Recent work of *Huang et al.* [2010] (their Figure 12h) also shows
139 that the typical dust height is much lower in winter (around 1-2 km) than summer (around
140 3-4 km). Thus, we choose 850-hPa instead of 700-hPa winds for the analysis results
141 presented here.

142 Figure 3 shows the composite maps of boreal winter MJO-related MODIS/Aqua
143 AOT anomalies (multiplied by 100 and with 95% confidence limits based on a Student's
144 t-test) and 850-hPa NCEP/NCAR horizontal wind anomalies over the tropical Atlantic
145 region (70°W-30°E, 20°S-30°N). In Figure 3 we see large AOT anomalies over the
146 equatorial Atlantic, collocated with the background aerosol plume (Figure 2). The highest
147 magnitude (±0.04) and largest latitudinal extent (~15°S - 20°N) of these AOT anomalies
148 are typically found over the eastern equatorial Atlantic along the west coast of Africa.
149 The AOT anomalies range up to about ±0.04 for the composite MJO and are about 20%
150 of their background mean (~0.2) (Figure 2). However, the AOT anomalies for individual
151 MJO events are about ±0.2 and can be as large as ±0.8. These AOT anomalies for
152 individual MJO events are much larger than MODIS AOT uncertainty (±0.03) [*Remer et*
153 *al.*, 2005; 2008] and comparable to the AOT anomalies caused by dust storms at synoptic
154 scale (~0.2) [*Wong et al.*, 2006]. To demonstrate the importance of the intra-seasonal
155 variations of the Atlantic aerosols in their overall variability, Figure 4 shows the standard
156 deviations of boreal winter AOT anomalies after removing the mean seasonal cycle (>= 2
157 days, total) (4a) and those for the intra-seasonal time scale after removing the mean
158 seasonal cycle and filtering via a 30–90-day band pass filter (note color scale change)
159 (4b) as well as the percentage of the total variance of boreal winter AOT anomalies
160 explained by their intra-seasonal variance (4c). The spatial patterns of the standard

161 deviations of boreal winter AOT anomalies for both total and intra-seasonal time scales
162 are similar to that of the mean AOT in Figure 2. The magnitude of the total standard
163 deviations is about half of that of the means. Furthermore, the magnitude of the intra-
164 seasonal standard deviation is about half of that of the total anomalous (apart from the
165 seasonal cycle) standard deviations. As is evident, the intra-seasonal variance accounts
166 for about 25% of the total variance of the aerosol variability over the tropical Atlantic
167 (e.g., 5°S-15°N). Thus, intra-seasonal variability, and even that part driven by the MJO,
168 is one of the most important forms of Atlantic aerosol variability.

169 For a comparison between the current MODIS/Aqua results and our earlier
170 MODIS/Terra results, the phases 2, 4, 6, and 8 in the current Figure 3 (hereafter CF3)
171 roughly correspond to the lags 0, +2, +4, and -2 in Figure 4 of *Tian et al.* [2008]
172 (hereafter OF4) according to the location of MJO convection (rainfall) anomalies (see
173 Figure 4 of *Tian et al.* [2008] and Figure 12 of *Waliser et al.* [2009]). Comparing these
174 two figures indicates that the general spatial and temporal patterns and magnitudes of
175 AOT anomalies over the Atlantic region are similar between MODIS/Aqua and
176 MODIS/Terra. For example, both phase 2 in CF3 and lag 0 in OF4 show strong negative
177 AOT anomalies over the tropical Atlantic when the enhanced convection is located over
178 the central and eastern equatorial Indian Ocean. In contrast, both phase 6 in CF3 and lag
179 +4 in OF4 show strong positive AOT anomalies over the tropical Atlantic when the
180 enhanced convection is located over the equatorial western Pacific. Furthermore, both
181 phase 4 in CF3 and lag +2 in OF4 show weak positive AOT anomalies over the tropical
182 North Atlantic and weak negative AOT anomalies over the tropical South Atlantic when
183 the enhanced convection is located over the Maritime Continent, and conversely for

184 phase 8 in CF3 and lag -2 in OF4. The global spatial and temporal patterns of
185 MODIS/Aqua and MODIS/Terra AOT anomalies are also similar (not shown).

186 Figure 3 also demonstrates the strong impact of low-level horizontal, especially
187 zonal, wind anomalies on the Atlantic AOT anomalies. For example, at phase 2 when the
188 enhanced convection is located over the central and eastern equatorial Indian Ocean
189 (Figure 12 of *Waliser et al.* [2009]), the 850-hPa horizontal wind anomalies over the
190 equatorial Atlantic are persistent westerlies that blow from the Atlantic Ocean to Africa
191 as a dynamical response to the enhanced convection over the Indian Ocean. These
192 westerly anomalies suppress the background westward aerosol transport by the low-level
193 mean easterlies and cause the negative AOT anomalies over the Atlantic region. A
194 similar argument can also be applied to phases 1 and 3. In contrast, in phase 6 when the
195 enhanced MJO convection is located over the equatorial western Pacific (Figure 12 of
196 *Waliser et al.* [2009]), the 850-hPa horizontal wind anomalies over the equatorial Atlantic
197 are persistent easterlies that blow from Africa to the Atlantic Ocean as a dynamical
198 response to suppressed convection over the Indian Ocean. These easterly anomalies
199 enhance the background westward aerosol transport by the low-level mean easterlies and
200 cause the positive AOT anomalies over the Atlantic region. Similar reasoning also
201 applies to phases 4 and 5. To better demonstrate the important role of low-level zonal
202 wind anomalies in the Atlantic AOT anomalies, Figure 5 shows the linear correlation
203 coefficient between the MODIS/Aqua AOT anomalies for the composite MJO cycle
204 (Figure 3) and 850-hPa NCEP/NCAR zonal wind anomalies for the composite MJO cycle
205 over the tropical Atlantic region. Here, negative (positive) correlation means that
206 westerly anomalies induce negative (positive) AOT anomalies or easterly anomalies

induce positive (negative) AOT anomalies. Clearly, the AOT anomalies are negatively correlated with the 850-hPa zonal wind anomalies over most part of tropical Atlantic and the west coast of Africa. The largest negative correlation (~ -0.9) is found over the south equatorial Atlantic and western Africa (10°S-EQ, 0°-30°E). These results indicate that the intra-seasonal aerosol variations over the tropical Atlantic are produced by the low-level zonal wind anomalies over the Atlantic associated with the MJO. In other words, the MJO modulates the Atlantic aerosols through its influence on the Atlantic low-level zonal wind anomalies and westward aerosol transport from Africa. It is also interesting to note a positive correlation between AOT and zonal wind over the east coast of South America around (15°S, 40°W) where the background trade winds blow the clean marine air from south Atlantic to South America (Figure 2). Thus, westerly (easterly) anomalies will reduce (enhance) the marine air input to the land and enhance (suppress) the local biomass burning activity and aerosol loading. The 700-hPa winds were also examined and the results are very similar those from 850 hPa.

4. Conclusions and discussion

This study aims to investigate the physical mechanism of large intra-seasonal variations in tropical Atlantic aerosols found in our previous study [*Tian et al.*, 2008] through analyzing the MODIS/Aqua AOT and NCEP/NCAR 850-hPa horizontal winds. First, through reference to our earlier study, we show that the general spatial and temporal patterns and magnitudes of AOT anomalies over the Atlantic region are similar between MODIS/Aqua and MODIS/Terra. The intra-seasonal variance related to the MJO accounts for about 25% of the total variance of MODIS/Aqua AOT over the tropical Atlantic. Thus, the intra-seasonal variability is one of the most important forms

230 of Atlantic aerosol variability. Second, we show that when enhanced MJO convection is
231 located over the equatorial Indian Ocean, persistent low-level westerly anomalies over
232 the equatorial Atlantic suppress the background westward aerosol transport and cause the
233 negative AOT anomalies over the Atlantic region. In contrast, when enhanced MJO
234 convection is located over the equatorial western Pacific, persistent low-level easterly
235 anomalies over the equatorial Atlantic enhance the background westward aerosol
236 transport and cause the positive AOT anomalies over the Atlantic region. These results
237 indicate that the intra-seasonal aerosol variations over the tropical Atlantic are produced
238 by the low-level zonal wind anomalies over the Atlantic associated with the MJO. In
239 other words, the MJO modulates the Atlantic aerosols through its influence on the
240 Atlantic low-level zonal wind anomalies and westward aerosol transport from Africa.
241 Given the potential predictability of the MJO extending to 2-4 weeks [e.g., *Waliser*,
242 2005], this study implies that components of the Atlantic aerosol concentration may be
243 predictable with lead times of 2-4 weeks, which in turn may lend important guidance to
244 the climate processes, such as air quality, dust storm, and ocean nutrients, over the
245 Atlantic Ocean. Furthermore, this study will provide an important physical/chemical
246 process to evaluate chemical transport models and help the model development.

247 **Acknowledgments**

248 This research was performed at Jet Propulsion Laboratory (JPL), California
249 Institute of Technology, under a contract with NASA. It was supported in part by the
250 Atmospheric Infrared Sounder (AIRS) project at JPL and the National Science
251 Foundation (NSF) grant ATM-0840755 at University of California, Los Angeles.

252

253

253 **References**

254 Cakmur, R. V., R. L. Miller, and I. Tegen (2001), A comparison of seasonal and
255 interannual variability of soil dust aerosols over the Atlantic Ocean as inferred by
256 the TOMS AI and AVHRR AOT retrievals, *J. Geophys. Res.*, *106*(D16), 18287-
257 18303.

258 Carlson, T. N., and J. M. Prospero (1972), The large-scale movement of Saharan air
259 outbreaks over the northern equatorial Atlantic, *J. Appl. Meteorol.*, *11*(2), 283-
260 297, doi:10.1175/1520-0450(1972)011<0283:TLSMOS>2.0.CO;2.

261 Chiapello, I., G. Bergametti, L. Gomes, B. Chatenet, F. Dulac, J. Pimenta, and E. S.
262 Suares (1995), An additional low layer transport of Sahelian and Saharan dust
263 over the north-eastern tropical Atlantic, *Geophys. Res. Lett.*, *22*(23), 3191-3194.

264 Huang, J. F., C. D. Zhang, and J. M. Prospero (2010), African dust outbreaks: A satellite
265 perspective of temporal and spatial variability over the tropical Atlantic Ocean, *J.*
266 *Geophys. Res.*, *115*, D05202, doi:10.1029/2009jd012516.

267 Husar, R. B., J. M. Prospero, and L. L. Stowe (1997), Characterization of tropospheric
268 aerosols over the oceans with the NOAA Advanced Very High Resolution
269 Radiometer optical thickness operational product, *J. Geophys. Res.*, *102*(D14),
270 16889-16909.

271 Kaufman, Y. J., D. Tanre, H. R. Gordon, T. Nakajima, J. Lenoble, R. Frouin, H. Grassl,
272 B. M. Herman, M. D. King, and P. M. Teillet (1997), Passive remote sensing of
273 tropospheric aerosol and atmospheric correction for the aerosol effect, *J.*
274 *Geophys. Res.*, *102*(D14), 16815-16830.

275 Kaufman, Y. J., I. Koren, L. A. Remer, D. Tanre, P. Ginoux, and S. Fan (2005), Dust
276 transport and deposition observed from the Terra-Moderate Resolution Imaging
277 Spectroradiometer (MODIS) spacecraft over the Atlantic ocean, *J. Geophys. Res.*,
278 *110*(D10), D10s12, doi:10.1029/2003jd004436.

279 Lau, W. K. M., and D. E. Waliser (Eds.) (2005), *Intraseasonal Variability of the*

280 *Atmosphere-Ocean Climate System*, 474 pp., Springer, Heidelberg, Germany.
281 Li, K.-F., B. Tian, D. E. Waliser, and Y. L. Yung (2010), Tropical mid-tropospheric CO2
282 variability driven by the Madden-Julian Oscillation, *Proc. Nat. Acad. Sci.*, in
283 press.
284 Madden, R. A., and P. R. Julian (1971), Detection of a 40-50 day oscillation in the zonal
285 wind in the tropical Pacific, *J. Atmos. Sci.*, *28*(7), 702-708.
286 Madden, R. A., and P. R. Julian (1972), Description of global-scale circulation cells in
287 tropics with a 40-50 day period, *J. Atmos. Sci.*, *29*(6), 1109-1123.
288 Remer, L. A., Y. J. Kaufman, D. Tanre, S. Mattoo, D. A. Chu, J. V. Martins, R. R. Li, C.
289 Ichoku, R. C. Levy, R. G. Kleidman, T. F. Eck, E. Vermote, and B. N. Holben
290 (2005), The MODIS aerosol algorithm, products, and validation, *J. Atmos. Sci.*,
291 *62*(4), 947-973.
292 Remer, L. A., R. G. Kleidman, R. C. Levy, Y. J. Kaufman, D. Tanre, S. Mattoo, J. V.
293 Martins, C. Ichoku, I. Koren, H. B. Yu, and B. N. Holben (2008), Global aerosol
294 climatology from the MODIS satellite sensors, *J. Geophys. Res.*, *113*(D14),
295 D14s07, doi:10.1029/2007jd009661.
296 Tanre, D., Y. J. Kaufman, M. Herman, and S. Mattoo (1997), Remote sensing of aerosol
297 properties over oceans using the MODIS/EOS spectral radiances, *J. Geophys.*
298 *Res.*, *102*(D14), 16971-16988.
299 Tian, B., Y. L. Yung, D. E. Waliser, T. Tyranowski, L. Kuai, E. J. Fetzer, and F. W. Irion
300 (2007), Intraseasonal variations of the tropical total ozone and their connection to
301 the Madden-Julian Oscillation, *Geophys. Res. Lett.*, *34*(8), L08704,
302 doi:10.1029/2007GL029451.
303 Tian, B., D. E. Waliser, R. A. Kahn, Q. Li, Y. L. Yung, T. Tyranowski, I. V.
304 Geogdzhayev, M. I. Mishchenko, O. Torres, and A. Smirnov (2008), Does the
305 Madden-Julian Oscillation influence aerosol variability?, *J. Geophys. Res.*,
306 *113*(D12), D12215, doi:10.1029/2007jd009372.

307 Tian, B., D. E. Waliser, E. J. Fetzer, and Y. L. Yung (2010), Vertical moist
308 thermodynamic structure of the Madden-Julian Oscillation in Atmospheric
309 Infrared Sounder retrievals: An update and a comparison to ECMWF interim
310 reanalysis, *Mon. Wea. Rev.*, *0*(0), doi:10.1175/2010MWR3486.1.
311 Waliser, D., K. Sperber, H. Hendon, D. Kim, M. Wheeler, K. Weickmann, C. Zhang, L.
312 Donner, J. Gottschalck, W. Higgins, I. S. Kang, D. Legler, M. Moncrieff, F.
313 Vitart, B. Wang, W. Wang, S. Woolnough, E. Maloney, S. Schubert, and W.
314 Stern (2009), MJO simulation diagnostics, *J. Climate*, *22*(11), 3006-3030,
315 10.1175/2008jcli2731.1.
316 Waliser, D. E. (2005), Predictability and forecasting, in *Intraseasonal Variability of the*
317 *Atmosphere-Ocean Climate System*, edited by W. K. M. Lau and D. E. Waliser,
318 pp. 389-424, Springer, Heidelberg, Germany.
319 Weare, B. C. (2010), Madden-Julian Oscillation in the tropical stratosphere, *J. Geophys.*
320 *Res.*, *115*, D17113, doi:10.1029/2009jd013748.
321 Wheeler, M. C., and H. H. Hendon (2004), An all-season real-time multivariate MJO
322 index: Development of an index for monitoring and prediction, *Mon. Wea. Rev.*,
323 *132*(8), 1917-1932.
324 Wong, S., P. R. Colarco, and A. E. Dessler (2006), Principal component analysis of the
325 evolution of the Saharan air layer and dust transport: Comparisons between a
326 model simulation and MODIS and AIRS retrievals, *J. Geophys. Res.*, *111*(D20),
327 D20109, doi:10.1029/2006jd007093.
328 Wong, S., and A. E. Dessler (2007), Regulation of H2O and CO in tropical tropopause
329 layer by the Madden-Julian oscillation, *J. Geophys. Res.*, *112*(D14), D14305,
330 doi:10.1029/2006JD007940.
331 Zhang, C. (2005), The Madden-Julian Oscillation, *Rev. Geophys.*, *43*, RG2003,
332 doi:10.1029/2004RG000158.
333 Ziemke, J. R., and S. Chandra (2003), A Madden-Julian Oscillation in tropospheric

ozone, *Geophys. Res. Lett.*, *30*(23), 2182, doi:10.1029/2003GL018523.

337 **Figure Captions**

338 **Figure 1:** (RMM1, RMM2) phase space for all days in boreal winter from November
339 2002 to April 2009 and the number of days for each phase of the MJO cycle.
340 Eight defined phases of the phase space are labeled to indicate the eastward
341 propagation of the MJO in one MJO cycle. Also labeled are the approximate
342 locations of the enhanced convective signal of the MJO for that location of the
343 phase space, e.g., the ''Indian Ocean'' for phases 2 and 3.

344 **Figure 2:** (a) Climatological mean (2002-2009) boreal winter (November-April)
345 MODIS/Aqua AOT and NCEP/NCAR 850-hPa horizontal winds over the
346 tropical Atlantic region. White regions indicate areas of missing MODIS/Aqua
347 AOT data. (b) As in (a) except for 700-hPa NCEP/NCAR horizontal winds.

348 **Figure 3:** Composite maps of boreal winter (November-April) MJO-related
349 MODIS/Aqua AOT anomalies (multiplied by 100) and NCEP/NCAR 850-hPa
350 horizontal wind (m s^{-1}) anomalies over the tropical Atlantic region. Only AOT
351 anomalies with above 95% confidence limit are shown.

352 **Figure 4:** (a) Standard deviation of boreal winter (November-April) MODIS/Aqua AOT
353 anomalies after removing the mean seasonal cycle (>= 2 days, total); (b) Same
354 as (a) except for intraseasonal time scale after removing the mean seasonal
355 cycle and filtering via a 30–90-day band pass filter; (c) Percentage of the total
356 variance of boreal winter MOIDS/Aqua AOT anomalies explained by their
357 intraseasonal variance.

358 **Figure 5:** Linear correlation coefficient between boreal winter (November-April) MJO-
359 related MODIS/Aqua AOT anomalies and NCEP/NCAR 850-hPa zonal wind

360 ($m\ s^{-1}$) anomalies over the tropical Atlantic region. Negative (positive)
361 correlation means that westerly anomalies induce negative (positive) AOT
362 anomalies or easterly anomalies induce positive (negative) AOT anomalies.
363

363

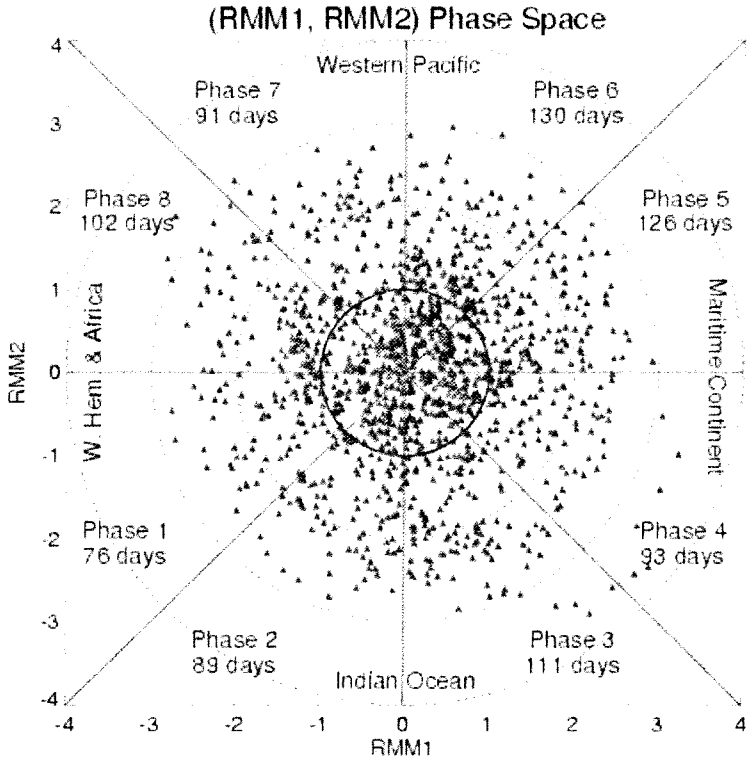

Figure 1: (RMM1, RMM2) phase space for all days in boreal winter from November 2002 to April 2009 and the number of days for each phase of the MJO cycle. Eight defined phases of the phase space are labeled to indicate the eastward propagation of the MJO in one MJO cycle. Also labeled are the approximate locations of the enhanced convective signal of the MJO for that location of the phase space, e.g., the ''Indian Ocean'' for phases 2 and 3.

364

365

365

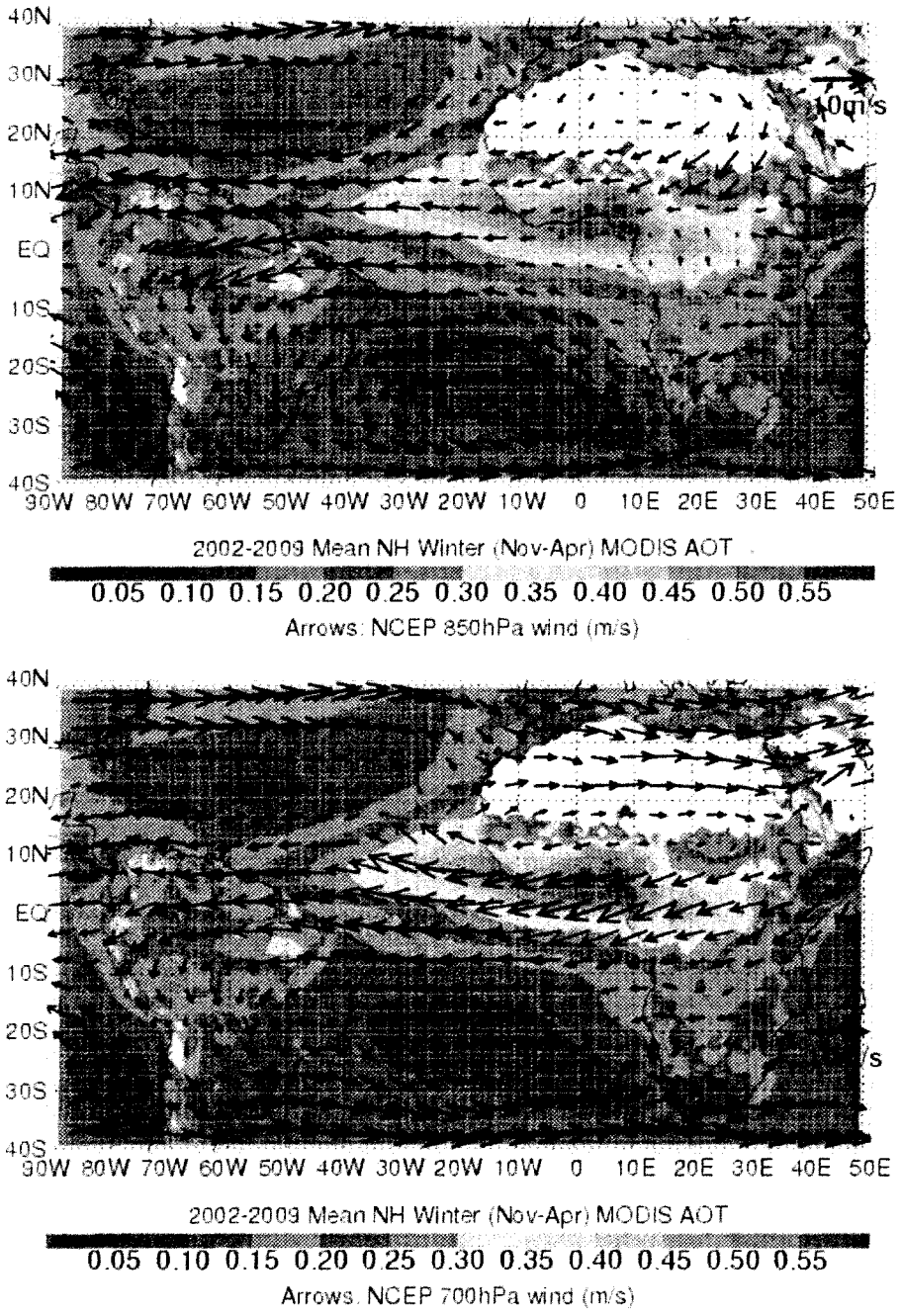

Figure 2: (a) Climatological mean (2002-2009) boreal winter (November-April) MODIS/Aqua AOT and NCEP/NCAR 850-hPa horizontal winds over the tropical Atlantic region. White regions indicate areas of missing MODIS/Aqua AOT data. (b) As in (a) except for 700-hPa NCEP/NCAR horizontal winds.

366

367

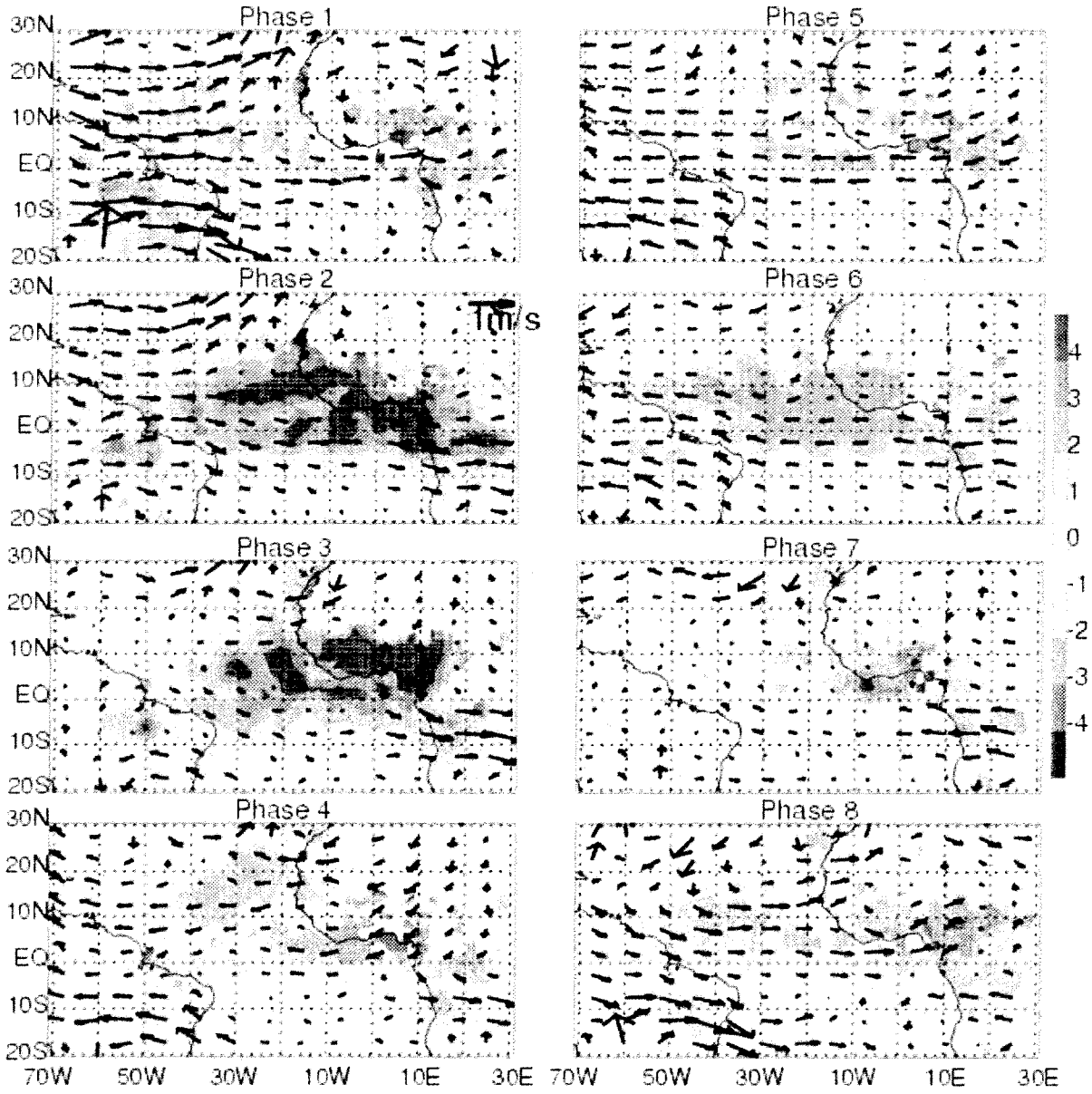

Figure 3: Composite maps of boreal winter (November-April) MJO-related MODIS/Aqua AOT anomalies (multiplied by 100) and NCEP/NCAR 850-hPa horizontal wind (m s^{-1}) anomalies over the tropical Atlantic region. Only AOT anomalies with above 95% confidence limit are shown.

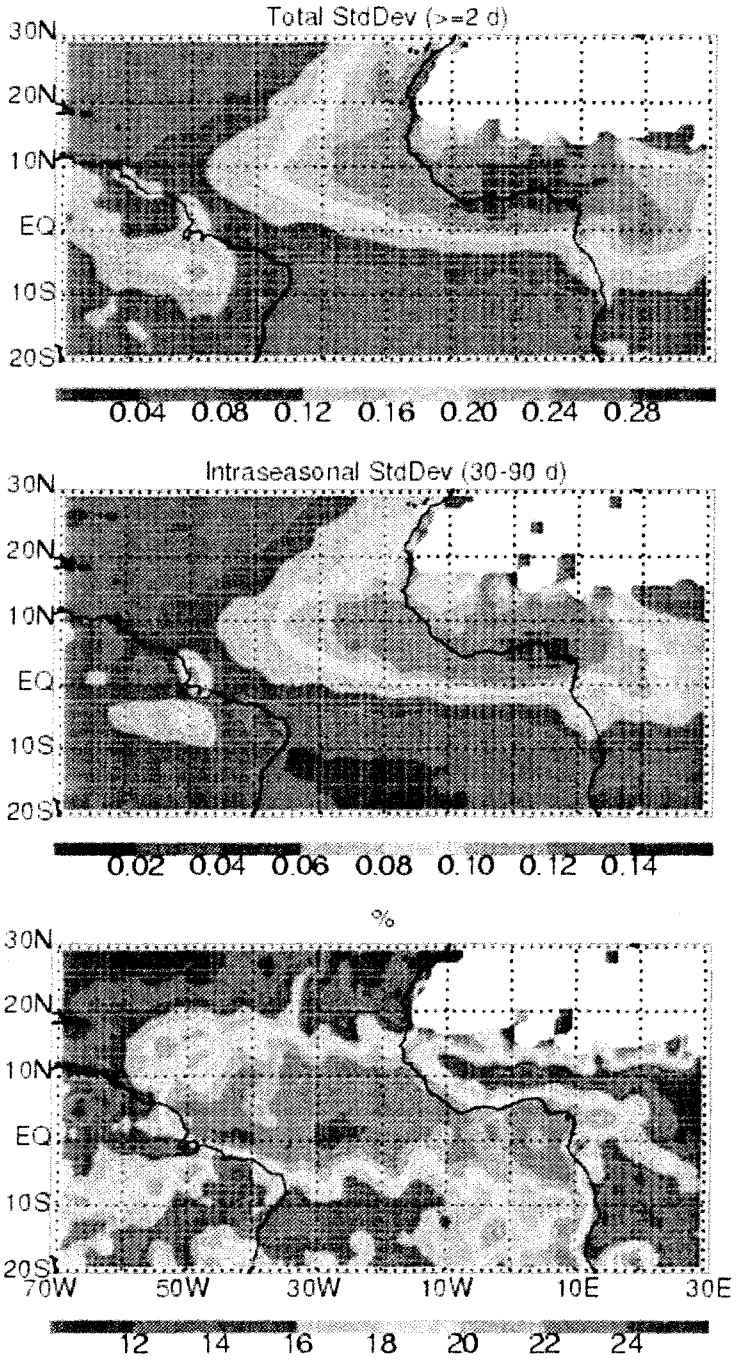

Figure 4: (a) Standard deviation of boreal winter (November-April) MODIS/Aqua AOT anomalies after removing the mean seasonal cycle (>= 2 days, total); (b) Same as (a) except for intraseasonal time scale after removing the mean seasonal cycle and filtering via a 30–90-day band pass filter; (c) Percentage of the total variance of boreal winter MOIDS/Aqua AOT anomalies explained by their intraseasonal variance.

377

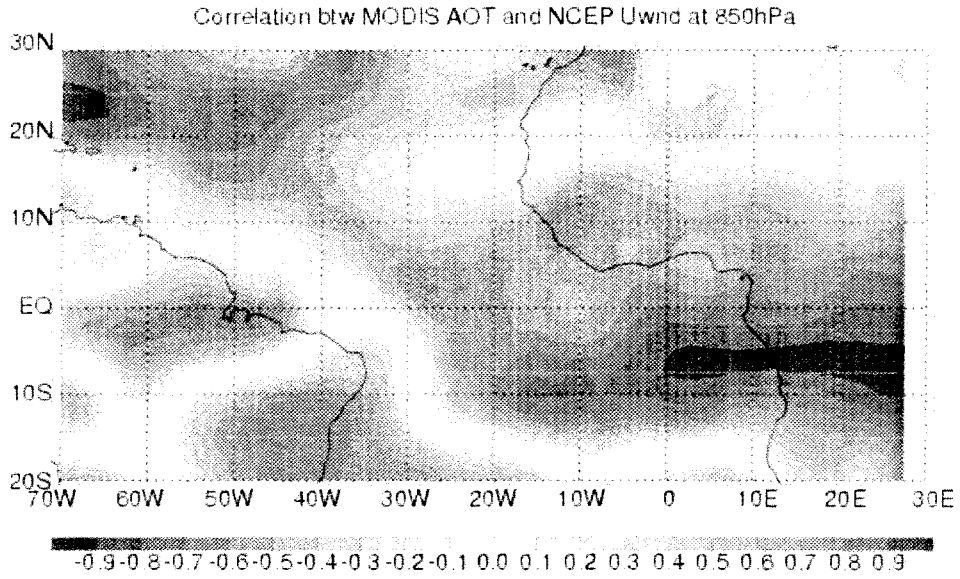

Figure 5: Linear correlation coefficient between boreal winter (November-April) MJO-related MODIS/Aqua AOT anomalies and NCEP/NCAR 850-hPa zonal wind (m s^{-1}) anomalies over the tropical Atlantic region. Negative (positive) correlation means that westerly anomalies induce negative (positive) AOT anomalies or easterly anomalies induce positive (negative) AOT anomalies.

378